Thesis for the Degree of Master of Science

Near-IR Polarimetry of The Star-Forming Regions around 30 Doradus

Jaeyeong Kim

School of Space Research
Graduate School
Kyung Hee University
Seoul, Korea

February, 2011

Near-IR Polarimetry of The Star-Forming Regions around 30 Doradus

Jaeyeong Kim

School of Space Research
Graduate School
Kyung Hee University
Seoul, Korea

February, 2011

Near-IR Polarimetry of The Star-Forming Regions around 30 Doradus

by

Jaeyeong Kim

advised by
Dr. Soojong Pak

Submitted to the School of Space Science
and Faculty of the Graduate School of Kyung Hee University
in partial fulfillment of the requirement for degree of
Master of Science

Dissertation Committee

……
Dr. Soojong Pak

……
Dr. Sungsoo S. Kim

……
Dr. Minho Choi

Near-IR Polarimetry of The Star-Forming Regions around 30 Doradus

ABSTRACT

The $20' \times 20'$ region around 30 Doradus in the Large Magellanic Cloud (LMC) were observed in the near-infrared wavelength using the Infrared Survey Facility 1.4 m telescope. We obtained polarimetry data in the *J*, *H*, and K_s bands using SIRIUS polarimeter, SIRPOL. We measured Stokes parameters of point-like sources to derive the degree of polarization and the polarization position angle. We examine the possible photometric errors to analyze polarization data for different aperture radii. To separate the Galactic foreground sources which can contaminate reliability of our polarimetric data, we apply methods to select the Galactic foreground sources. Color-magnitude diagram and proper motions for the sources are discussed as the methods, but color-magnitude diagram cannot show any significant difference with the main LMC sources. We conclude that the proper motion is more reliable to extract the embedded sources in the foreground stars. These data reduction and the analysis methods will be applied to the large area survey data in the LMC.

Table of Contents

1. INTRODUCTION

Magnetic fields are an important component of the interstellar medium. They channel gas flows, accelerate and distribute energy from cosmic rays, and may be a significant component of the galactic pressure, especially in low mass galaxies (Kepley 2009).

One of the orientation mechanisms (Davis & Greenstein 1951) produces grain alignment with respect to magnetic field, even if the alignment mechanism is of non-magnetic nature. This alignment is true due to the rapid precession of grains about magnetic field. This precession stems from the substantial magnetic moment that grains get due to their rotation (Dolginov & Mytrophanov 1976). In molecular clouds, dust grains get aligned with respect to magnetic field as they tend to be aligned with their long axes perpendicular to magnetic field. This mechanism is based on the direct interaction of rotating grains with the interstellar magnetic field (Lazarian 2006). Polarization of starlight may arise from absorption and scattering by elongated dust grains that are at least partially aligned by magnetic fields (Davis & Greenstein 1951). The magnetic field direction can be measured by observing the dichroic polarization of background stars in the optical and near-IR bands and/or the linearly polarized emission from the aligned dust grains in the mid-IR and far-IR bands (Kandori et al. 2007). Dichroism is the differential extinction of orthogonally polarized radiation components, because interstellar dust particles are non-spherical (Tinbergen 1996).

The Large Magellanic Cloud (LMC) is one of the nearest extragalaxies. The interstellar medium of the LMC has quite different properties from those of our Galaxy, e.g., a lower metallicity and different dust properties (Pak et al. 1998; Nakajima et al. 2007). The LMC has revealed the presence of large-scale magnetic fields (Gaensler et al. 2005). Optical polarization observations (Schmidt 1970, 1976; Mathewson and Ford 1970) showed a regular polarization distribution. Wayte (1990) showed that the magnetic field threads both LMC and the Small Magellanic Cloud (SMC). The 30 Doradus is a

unique, giant star formation complex in the LMC and is centered on a dense, massive cluster of newly formed stars. The level of star formation exhibited by the 30 Doradus region and the neighboring the LMC complex are the closest examples of starburst-type star formation (Walborn \& Blades 1997; Brandner et al. 2001; Maercker \& Burton 2005). Furthermore, this nebula plays a key role in the understanding of HII regions (Scowen et al. 2009). Multi-frequency radio continuum surveys (Haynes et al. 1991) showed that there are filamentary magnetic fields in the LMC. The fields seem to be associated with the 30 Doradus and not with the main body of the LMC. Previous polarimetric observation and study about the 30 Doradus were presented by Nakajima et al. (2007).

For the study of the magnetic field in the LMC, the separation of the Galactic foreground sources are essential. In this paper, we present the results of near-infrared (NIR) polarimetric observations of a larger region around 30 Doradus. Section 2 describes the observations. Also in this section, data reduction processes, such like photometry and calculation of the Stokes parameters, are introduced. The study about photometry with different aperture radii and the comparing with previous data are mentioned to reduce the reliable data in Section 3. In Section 4, we discuss the methods for source classification to extract the Galactic foreground sources, such like Color-magnitude diagram and proper motions.

2. OBSERVATIONS AND DATA REDUCTION

2.1 Observations

The observations were carried out from 2008 December 25 to 30 with NIR wide-field polarimeter SIRPOL on the Infrared Survey Facility (IRSF) 1.4 m telescope at the South African Astronomical Observatory. Using the infrared camera SIRIUS which has three 1024 × 1024 HgCdTe infrared detector and provides simultaneous three-band images (Nagayama et al. 2003), we could obtain 5×9 regions in the LMC. We used near-infrared wavelengths to observe that regions; wavelengths are J (λ = 1.25μm), H (1.63 μm), and K_s (2.14μm) bands. SIRPOL enables us to obtain wide-field (7.7′ × 7.7′) polarimetric image with a scale of 0.45″ pixel^{-1}. See Kandori et al. (2006) for the details of SIRPOL. We performed 20 second exposures at four wave-plate angles (0°, 45°, 22°.5, and 67°.5) and at 10 dithered positions for one set. One set observation was performed at each frame. The total integration time was 200 second per wave-plate angle. Overall seeing size during the observations was ~1″.3 at J band, but we experienced unstable seeing conditions during nights. We selected 3×3 regions (20′ x 20′), around 30 Doradus, and present our initial investigation. Those regions are described in Table 1 and Figure 1.

2.2 Data Reduction

We used IRAF (Image Reduction & Analysis Facility) software package to reduce the data, e.g, dark-field subtraction, flat-field correction, median sky subtraction, and frame registration (Kandori et al. 2006). For source detection and photometry on Stokes I images, we used the IRAF daophot package (Stetson 1987). We detected stars having peak intensity greater than 10σ above the local sky background. We measured the instrumental magnitudes of stars by aperture photometry. The pixel coordinates of the detected sources were matched to celestial coordinates of their counter parts in the Two

Micron All Sky Survey (2MASS) Point Source Catalogue. The magnitude and color of our photometry were transformed to the 2MASS system using:

$$MAG_{2MASS} = MAG_{IRSF} + \alpha_1 \times COLOR_{IRSF} + \beta_1, \quad (1)$$

$$COLOR_{2MASS} = \alpha_2 \times COLOR_{IRSF} + \beta_2, \quad (2)$$

where MAG_{IRSF} is the instrumental magnitude from the IRSF images and MAG_{2MASS} is the magnitude from the 2MASS All Sky Point Source Catalogue. We calculated the Stokes parameters, I, Q, and U, the polarization degree, P, and the polarization position angle, θ, as below:

$$I = (I_0 + I_{22.5} + I_{45} + I_{67.5}) / 2, \quad (3)$$

$$Q = I_0 - I_{45}, \quad (4)$$

$$U = I_{22.5} - I_{67.5}, \quad (5)$$

$$P_\circ = \frac{\sqrt{Q^2 + U^2}}{I}, \quad (6)$$

$$\theta = \frac{1}{2}\arctan\frac{U}{Q}. \quad (7)$$

Since the initial polarization degree, $P_\circ$, is a positive quantity, the derived $P_\circ$ values tend to be overestimated, especially for low signal-to-noise ratio (S/N) sources. To correct for the bias, we use the following equation to calculate the debiased polarization degree:

$$P = \sqrt{P_\circ^2 - \delta P_\circ^2}, \quad (8)$$

where $\delta P_\circ$ is the error in $P_\circ$ (Wardle & Kronberg 1974). The polarization efficiencies of SIRPOL (95.5, 96.3, and 98.5% at J, H, and K_s bands, respectively) were used for correcting debiased polarization degree (Kandori et al. 2006).

3. RESULTS

3.1 Photometry with Aperture Radius of 4 Pixels

In the photometry processes, most of the previous SIRPOL data have used an aperture radius of 4 pixels. But considering our insufficient exposure time, 200 second for each wave-plate angle, this size could be too small to obtain sufficient photons from the sources. In bad weather conditions, the variable seeing can produce systematic polarization patterns.

Our photometry with aperture radius of 4 pixels and sky annulus of 10 pixels detected 2669 sources in JHK_s bands over the entire regions. In these sources, the sources which had $P \geq 3\sigma_P$ were considered and examined polarization result with the polarization vector map. The vector maps with an aperture radius of 4 pixels are represented in Figure 2. As shown in this figure, each region do not seem to show correlation with each side of region. In other words, the nine regions seem to have systematic patterns about the polarized sources which are included in each region.

3.2 Photometry with Aperture Radius of 8 and 12 Pixels

While it is usual to use an aperture radius of 4 pixels, it is necessary to verify the results when the quality of images is worse than the usual. To verify our results, we performed the analysis again using larger aperture radius. We set aperture radius to 8 and 12 pixels and sky annulus to 13 pixels, and executed photometry and polarimetry again. We investigated the relation between the aperture radius and the polarization results. We select the sources which are matched at each result for different aperture radii (i.e, the sources were included in the results by aperture radius of 4, 8, and 12 pixels.).

Figure 3 represents the polarization degree ratios of the aperture radius of 4 and 8 pixels to the aperture radius of 12 pixels. The ratio of 4 to 12 pixels has higher value than

the ratio of 8 to 12 pixels. This result implies that the photometry data of the aperture radius of 4 pixels can be significantly affected by the seeing variations during observations. Also we need to note that the polarization degrees become slightly higher as an aperture radius was increased.

We also compared the polarization angles between the different aperture radii as shown in Figure 4. There are tight correlations between aperture radius of 8 pixels and aperture radius of 12 pixels, contrary to the ratio of 4 pixels to 12 pixels. This result means that polarization angles of aperture radius of 8 pixels are very reliable. Although the larger aperture makes higher photometric noise, we decide to use aperture radius of 8 pixels for further discussions.

From these processes, we dealt with data which set aperture radius to 8 pixels and derived polarization degree and angle of 2562 sources. But we considered meaningful stars with $P \geq 3\sigma_P$. Numbers of selected stars of entire regions are 736, 784, and 427 stars at J, H, and K_s, respectively. Figures 5 shows polarization vector map with an aperture radius of 8 pixels. These maps show a different distribution from the maps with an aperture radius of 4 pixels. The maps whose set aperture radius to 8 pixels did not show discrete trend of polarization angles. The differences between aperture radius 4 and 8 pixels imply that improper photometry environments can occur systematic errors in polarimetry. Figure 6 shows the distributions for polarization degrees and angles in nine fields with aperture radius of 8 pixels.

3.3 Comparing with Previous Results

To make sure our results, we compare our data with previous observations. Nakajima et al. (2007, hereafter N07) would be a standard for this verification in the central regions of the 30 Doradus. N07 observed the 30 Doradus field centered at $(\alpha, \delta)_{2000} = (5^h38^m45^s, -69^\circ05'29'')$, but our 30 Doradus field (region n5 in Table 1.) is centered at $(\alpha, \delta)_{2000} = (5^h38^m34.48^s, -69^\circ06'02.2'')$. Because of this difference in the centers, we could not

compare both data exactly. In addition, our photometry in the 30 Doradus are limited by the nebula features, while N07 showed many photometry sources with long exposure data, i.e., total of 1480 second per wave-plate angle.

The numbers of the matched sources in both data are 33, 36, and 7 at *J*, *H*, and K_s bands, respectively. With these sources, we compared polarization degree and angle (Figure 7). Figure 8 shows that N07 and our data have a similar tendency at this graph.

4. DISCUSSION

Source classification is important to understand properties of stars as well as to separate the Galactic foreground sources and the sources from those in the LMC. The Galactic foreground sources can contaminate polarimetry result by their intrinsic polarization or are arisen calibration error by the sources which did not produce polarization itself. In this section, we applied two methods to test the separation reliabilities.

4.1 Color-Magnitude Diagram

The typical classification method is to use color-magnitude diagrams (hereafter *CM* diagrams). We followed the classification of Nikolaev & Weinberg (2000) and used criteria (in Table 2 of Nikolaev & Weinberg 2000) to separate sources. They denoted that the Galactic disk dwarfs of spectral classes in the range from late F to early K were distributed over foreground of the LMC. However, they only used the 2MASS samples with $m_{Ks} < 14$ mag. Our photometry data are available to $m_{Ks} < 16$ mag which mostly belongs to *group D* in Nikolaev & Weinberg (2000). Total five populations of stars are classified. Kato et al. (2007) also used criteria of Nikolaev & Weinberg (2000), but did not classify *group D*. Figure 9 represents the five groups. These groups can be represented by stellar population around the 30 Doradus as follows:

Group A: the main sequence;

Group EFG: the red-giant branch (RGB) and the early asymptotic giant branch (E-AGB);

Group B: the Galactic foreground sources;

Group I: Super giant and red clump; and

Group JK: the asymptotic giant branch (AGB) stars.

In these five groups, *Group A* and *Group I* can be confused to divide to the Galactic foreground and the main LMC sources. *Group JK* have dusty AGB stars which may have their own polarization by the shrouded dust (Parthasarathy & Jain 1993). The main focus is to compare *Group B* as the foreground sample and *Group EFG* which contain the main LMC stars. Because the classification of Nikolaev & Weinberg (2000) only used the 2MASS sources with $m_{Ks} < 14$ mag, we extrapolate the boundaries of the criteria regions up to $m_{Ks} < 16$ mag and plot the histograms for the sources in *Group B* and *Group EFG*. Figure 10 shows data in these regions. Figures 11 and 12 show the distributions for polarization degrees and angles of both *Group B* and *Group EFG*. From these results, we cannot find any significant difference between *Group B* and *Group EFG*. We conclude that *CM* diagram is not proper separation method, because the vague boundary lines of the foreground group cannot separate the Galactic foreground sources from the main LMC sources precisely.

4.2 Proper Motion

Vieira et al. (2010) investigated the proper motion in the Magellanic Clouds in the Southern Proper Motion (SPM) program. They used the resulting catalog of 1.4 million objects to derive the mean absolute proper motions of the LMC and the SMC. We used this catalog and examined proper motions to separate the foreground sources which are contained in our observed regions.

Total 805 sources were matched with SPM sources at JHK_s bands. Unfortunately, the sources which are detected in our nine fields have proper motions with significant errors.

Vieira et al. (2010) also discarded an area of high stellar density, at 71° ≤ α ≤ 76° and -68° ≤ δ ≤ -71°, with CCD data close to the LMC center. We verified that the sources in our nine fields appeared some relations between proper motion and polarization data. To avoid uncertainty of data, we used data which had proper motion $\mu > 3\sigma_\mu$ to select the Galactic foreground stars. μ is calculated as below.

$$\mu = \sqrt{(\mu_\alpha \cos\delta)^2 - \mu_\delta^2} \quad (9)$$

For the sources which have proper motion for $\mu < 3\sigma_\mu$ and $P \geq 3\sigma_P$, we examined their distributions for polarization degrees and angles to compare with the Galactic foreground sources. The sources which have $\mu > 3\sigma_\mu$ have the random distribution of polarization angle at each band. The sources which have $\mu < 3\sigma_\mu$ show the similar distribution of polarization angle at each band. We present these results in Figures 13~15. From these results, we can select the Galactic foreground stars in our field and suggest that polarization properties of stars can be related to their proper motions.

5. SUMMARY

We conducted investigation to solve systematical problem. Using different aperture radii, we examined the correlation between aperture radius and polarimetry result. Consequently we concluded to use aperture radius of 8 pixels with annulus of 13 pixels for photometry and polarimetry.

Considering insufficient exposure time, 200 second for each wave-plate angle, and unstable seeing condition, our aperture radius to perform photometry and polarimetry is reliable to set 2~3 times than usual aperture radius. We used the comparison data to make sure our results. Comparing with the sources of N07, we found that there are no significant differences in the polarimetry data of our sources.

We applied methods to select the Galactic foreground sources which can contaminate polarimetry result by their intrinsic polarization or arise calibration error by the sources which did not produce polarization itself. Using *CM* diagram, we selected the group which contained the foreground sources. But in the distributions for polarization degrees and angles, it did not have significant differences comparing with the main LMC sources. We also selected the Galactic foreground sources to use proper motion. The sources which are located in the foreground had significant value for proper motion, contrary to the main LMC sources. Although proper motion data had significant errors, we can separate the Galactic foreground sources from the main LMC sources. They showed the different distributions for polarization degrees and angles comparing with the main LMC sources.

Acknowledgments

This research was supported by WCU(World Class University) program through the National Research Foundation of Korea funded by the Ministry of Education, Science and Technology (R31-10016).

REFERENCES

Davis, L. J. & Greenstein, J. L. 1951, ApJ, 114, 206

Dolginov, A. Z. & Mytrophanov, I. G. 1976, Ap&SS, 43, 291

Gaensler, B. M., Haverkorn, M., Staveley-Smith, L., Dickey, J. M., McClure-Griffiths, N. M., Dickel, J. R., & Wolleben, M. 2005 Science 307, 1610

Haynes, R. F. et al. 1991, A&A 252, 475

Kandori, R. et al. 2006, Proc. SPIE, 6269, 159

Kandori, R. et al. 2007, PASJ, 59, 487

Kato, D. et al. 2007, PASJ, 59, 487

Kepley, A. A., Mühle S., Wilcots, E. M., Everett, J., Zweibel, E., Robishaw, T., and Heiles, C. 2007, IAUS, 259, 555

Lazarian, A. 2006, Astro.ph, 8049

Mathewson, D. S. & Ford, V. L. 1970, ApJ, 160, L43

Nakajima, Y. et al. 2007 PAFJ, 59, 519

Nagayama, T. et al. 2003, Proc. SPIE, 4841, 459

Nikolaev, S. & Weinberg, M. D. 2000, ApJ, 542, 804

Pak, Soojong, Jaffe, Daniel. T., van Dishoeck, Ewine F., Johansson, L. E. B., Booth, R. S.

1998, ApJ, 498, 735

Parthasarathy, M. & Jain, S. K. 1993, IAUS, 155, 353

Schmidt, Th., 1970, A&A, 6, 294

Schmidt, Th., 1976, A&A, 24, 357

Scowen, P. et al. 2009, Astro, 266

Stetson, P. B. 1987, PASP, 99, 191

J. Tinbergen: Dichroism. In: Astronomical Polarimetry, (Camebridge University press, 1996) pp 42

Vieira, K. et al., 2010, AJ, 140, 1934

Wardle, J. F. C. & Kronberg, P. P., 1974, ApJ, 194, 249

Wayte, S. R., 1990, ApJ, 355, 473

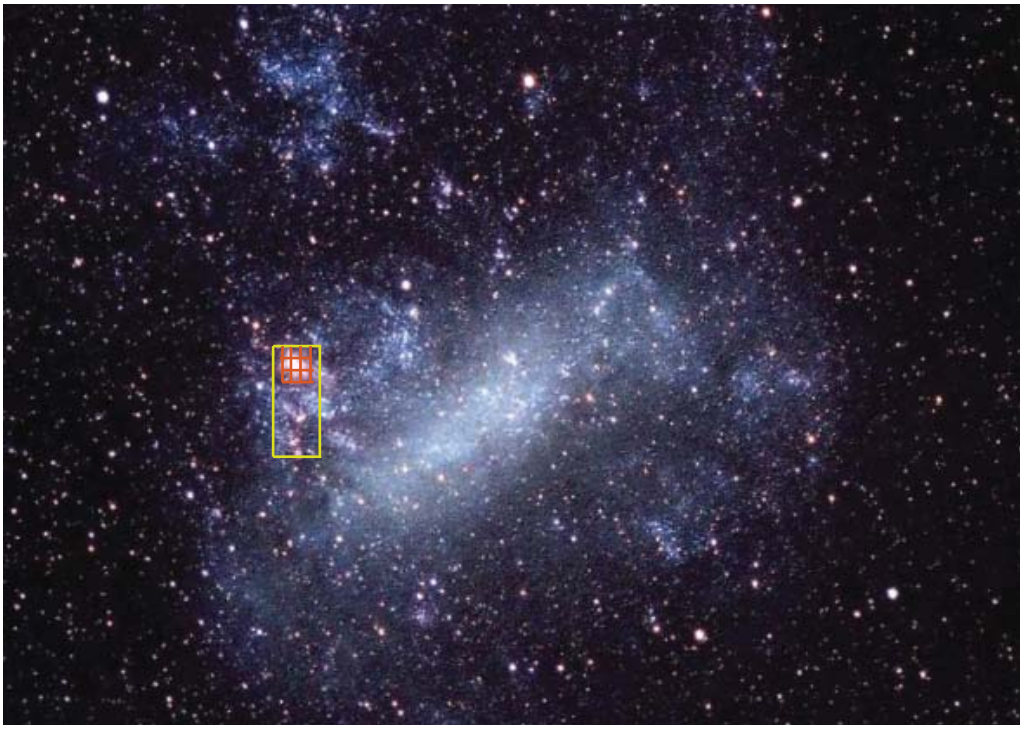

Fig. 1. The survey area of our observed 5×9 regions(yellow box) and around 30 Doradus regions(red box). This optical image offered by Mr. Kamiya.

Table 1. Observation log

Date	Field name	α_{J2000}	δ_{J2000}	Seeing in J band[″]
12/30/2008	n1	05 39 47.92	-68 59 09.9	1.2
	n2	05 38 33.53	-68 59 07.7	1.3
12/25/2008	n3	05 37 19.27	-68 59 03.9	1.3
	n4	05 37 19.86	-69 06 03.3	1.4
	n5	05 38 34.48	-69 06 02.2	1.4
	n6	05 39 48.78	-69 06 02.6	1.3
	n7	05 39 48.17	-69 12 38.0	1.3
	n8	05 38 32.91	-69 12 34.0	1.2
	n9	05 37 17.79	-69 12 32.4	1.3

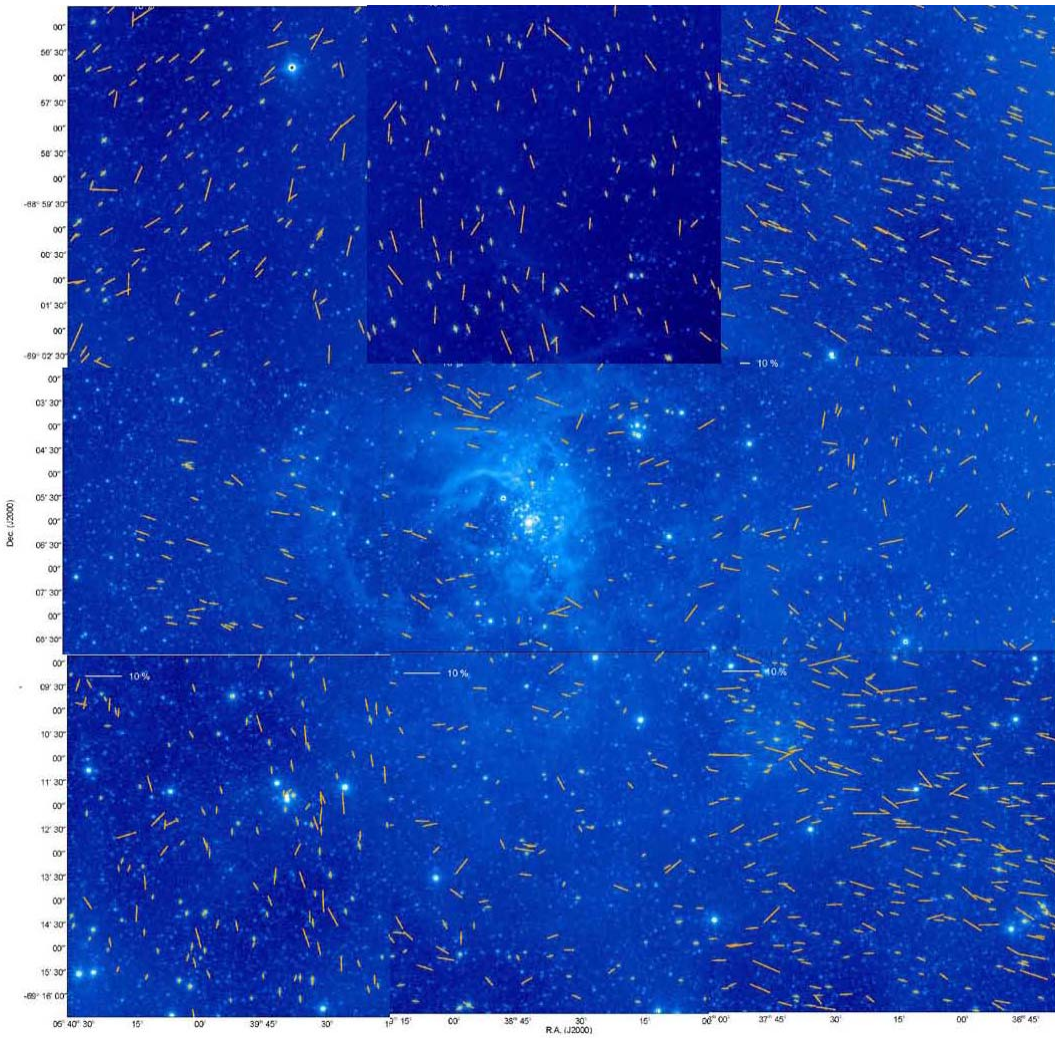

Fig. 2. Intensity images and polarization vectors (orange lines) of the polarized sources with $P \geq 3\sigma_P$ for the H band with aperture radius of 4 pixels. The length of vectors indicates the polarization degree (%).

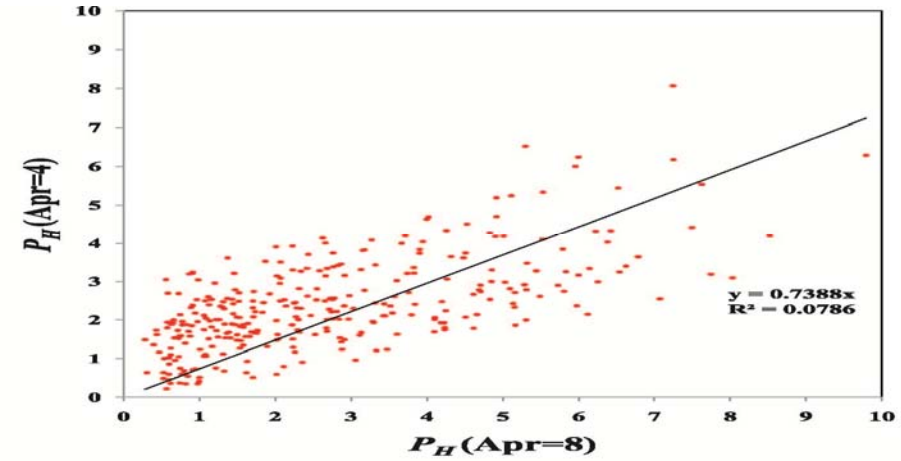
P_H(Apr=4)
P_H(Apr=8)
y = 0.7388x
R² = 0.0786

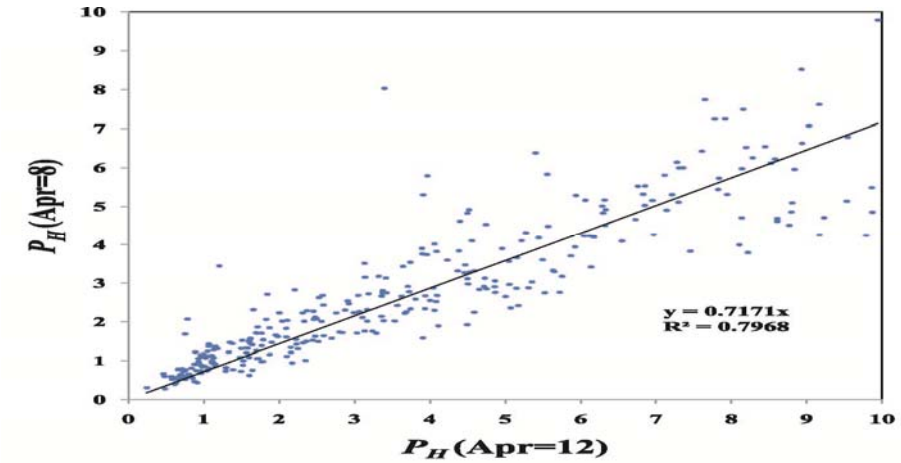
P_H(Apr=8)
P_H(Apr=12)
y = 0.7171x
R² = 0.7968

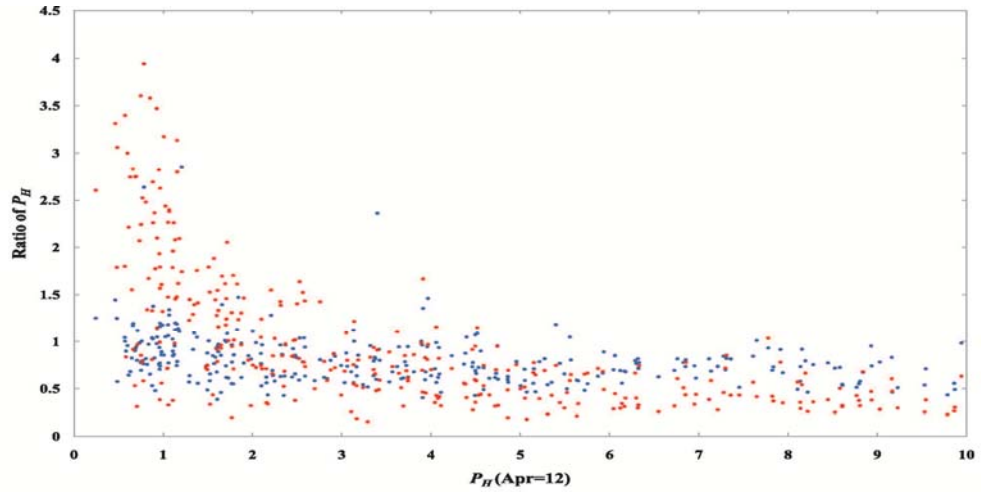
Ratio of P_H
P_H(Apr=12)

Fig. 3. (Top) Correlation plots of polarization degrees for different aperture radii (Aperture=4 vs. Aperture=8 pixels) less than 10% for the *H* band. (Middle) Correlation plots of polarization degrees for different aperture radii (Aperture=8 vs. Aperture=12 pixels) less than 10% for the *H* band. (Bottom) Correlation plots of the ratios of polarization degrees of aperture=4 to aperture=12 pixels and aperture=8 to aperture=12 pixels for the *H* band. The red plots indicate the ratios of aperture=4 to aperture=12 pixels and the blue plots indicate the ratios of aperture=8 to aperture=12 pixels.

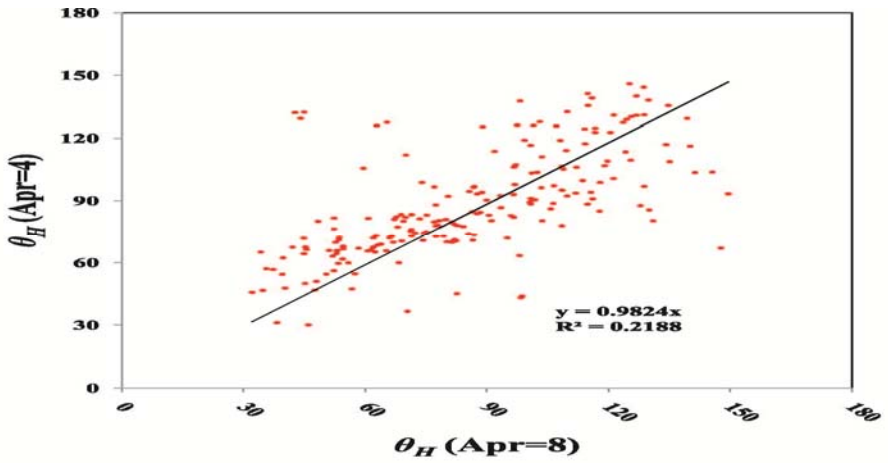
180
150
120
90
60
30
0
θ_H (Apr=4)
y = 0.9824x
R² = 0.2188
0
30
60
90
120
150
180
θ_H (Apr=8)

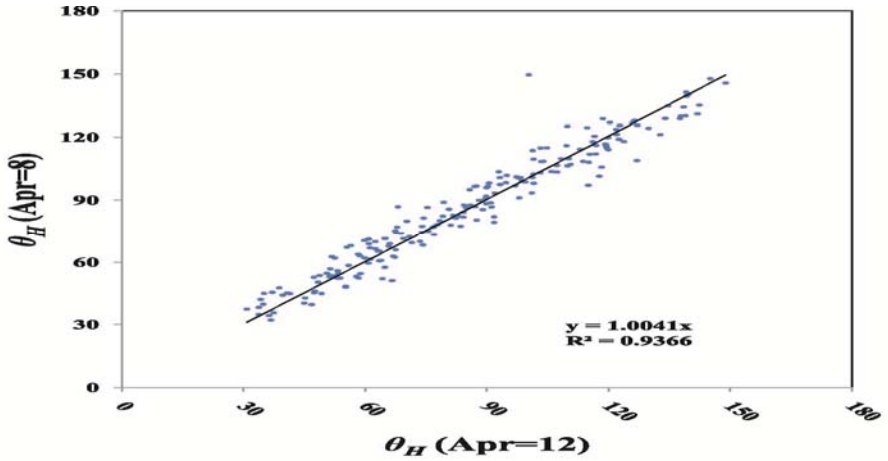
180
150
120
90
60
30
0
θ_H (Apr=8)
y = 1.0041x
R² = 0.9366
0
30
60
90
120
150
180
θ_H (Apr=12)

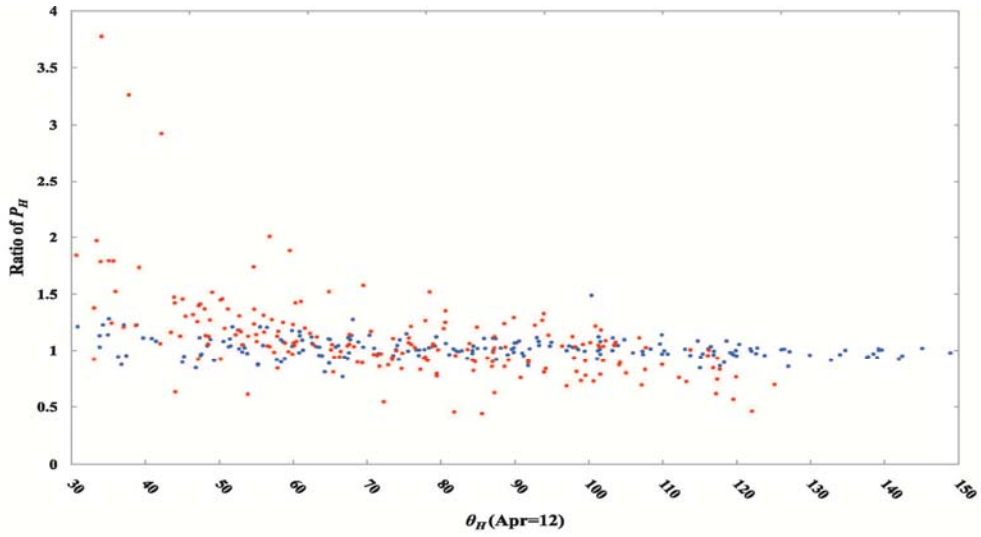
4
3.5
3
2.5
2
1.5
1
0.5
0
Ratio of P_H
30
40
50
60
70
80
90
100
110
120
130
140
150
θ_H(Apr=12)

Fig. 4. (Top) Correlation plots of polarization angles for different aperture radii (Aperture=4 vs. Aperture=8 pixels) between the range 30˚and 150˚ for the *H* band. (Middle) Correlation plots of polarization angles for different aperture radii (Aperture=8 vs. Aperture=12 pixels) between the range 30˚ and 150˚ for the *H* band. (Bottom) Correlation plots of the ratios of polarization angles of aperture=4 to aperture=12 pixels and aperture=8 to aperture=12 pixels for the *H* band. The red plots indicate the ratios of aperture=4 to aperture=12 pixels and the blue plots indicate the ratios of aperture=8 to aperture=12 pixels.

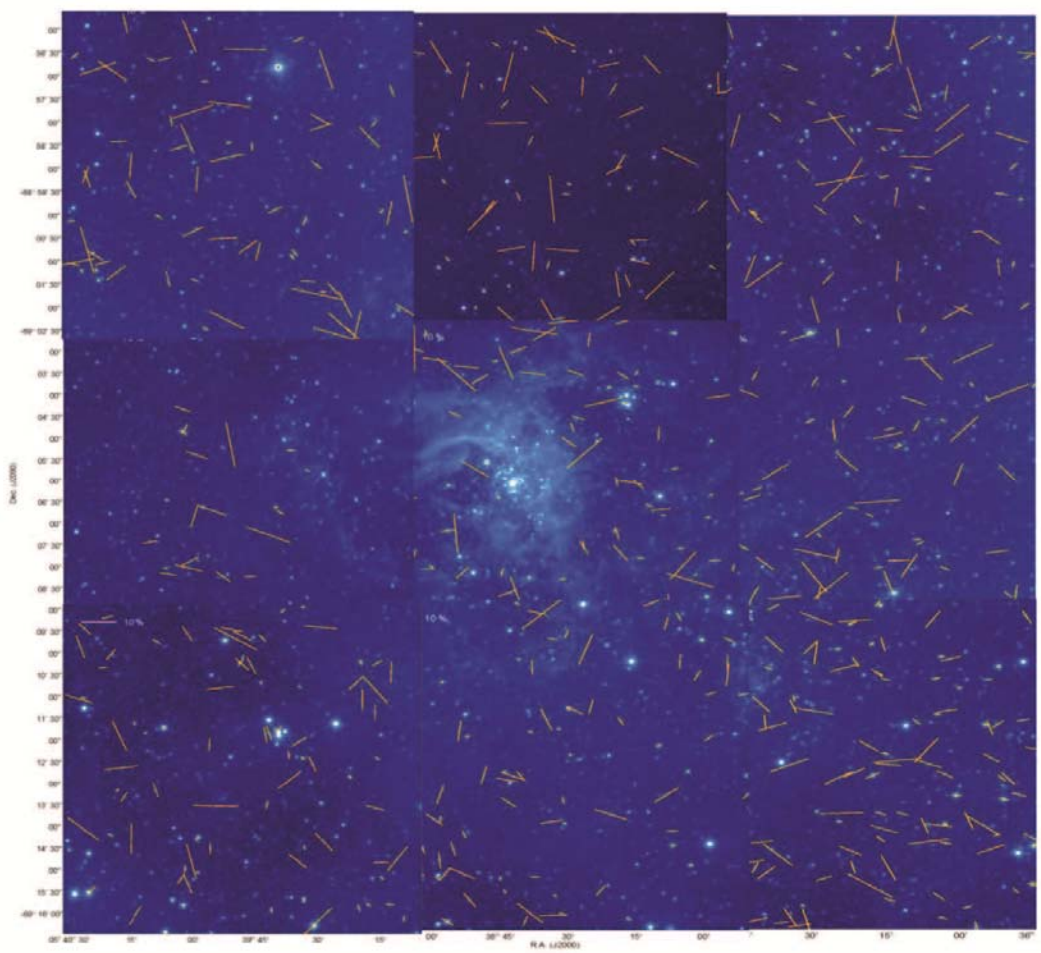

Fig. 5. Intensity images and polarization vectors (orange lines) of the polarized sources with $P \geq 3\sigma_P$ for the H band with aperture radius of 8 pixels. The length of vectors indicates the polarization degree (%).

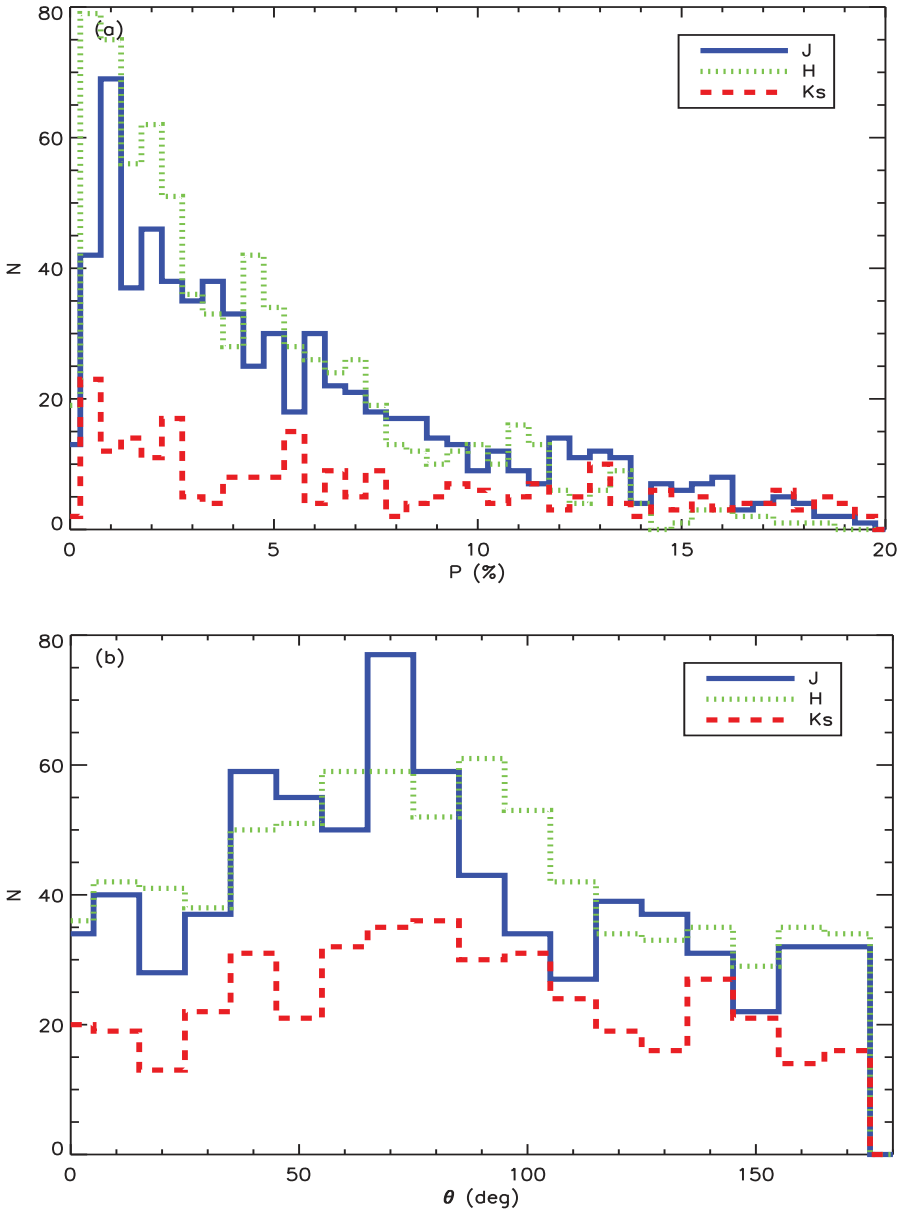

Fig. 6. (a) Histograms of polarization degree of the sources in nine fields with $P \geq 3\sigma_P$ for the J, H, K_s bands. (b) Histograms of polarization angle of the sources in nine fields with $P \geq 3\sigma_P$ for the the J, H, K_s bands.

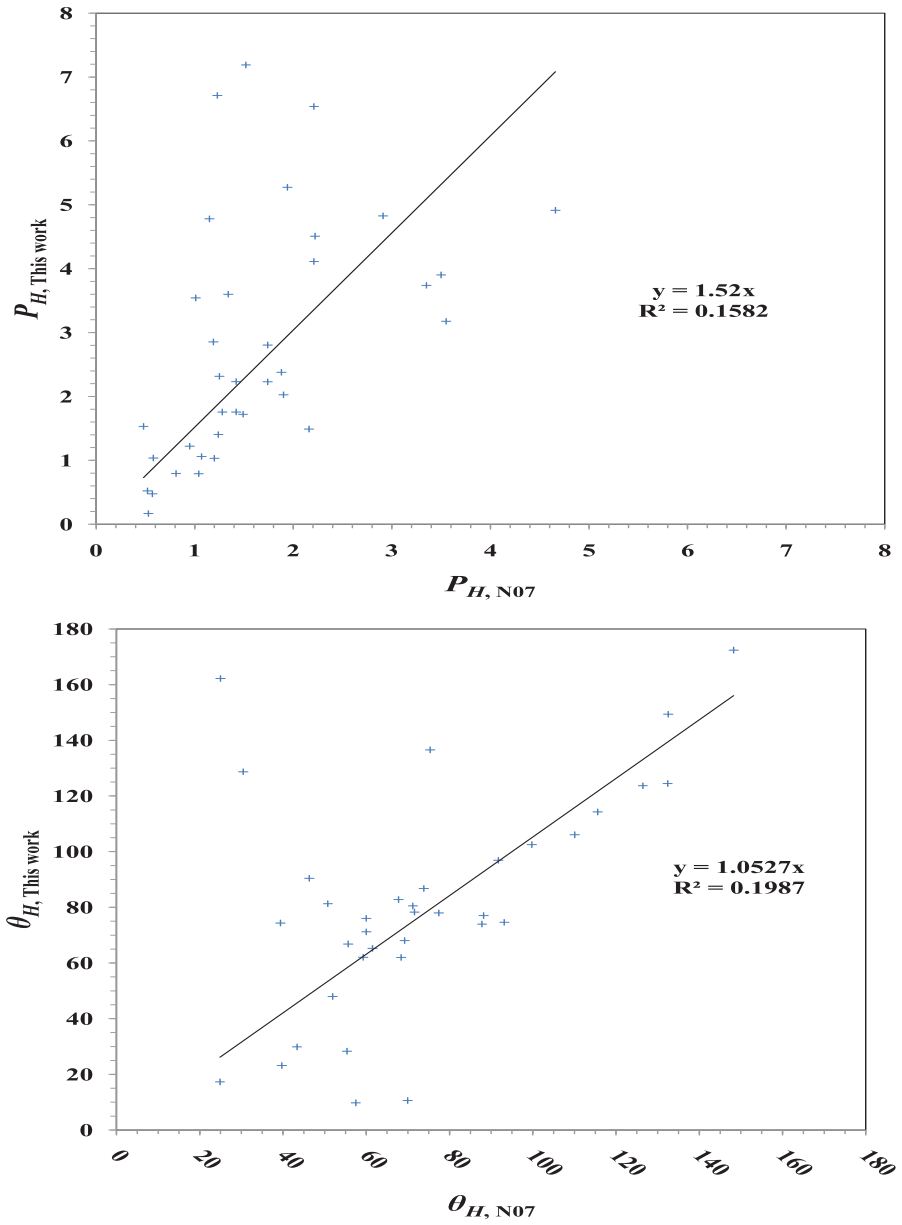

Fig. 7. Correlation graph of both matched data at *H* band. Polarization degree (left) and angle (right) are represented.

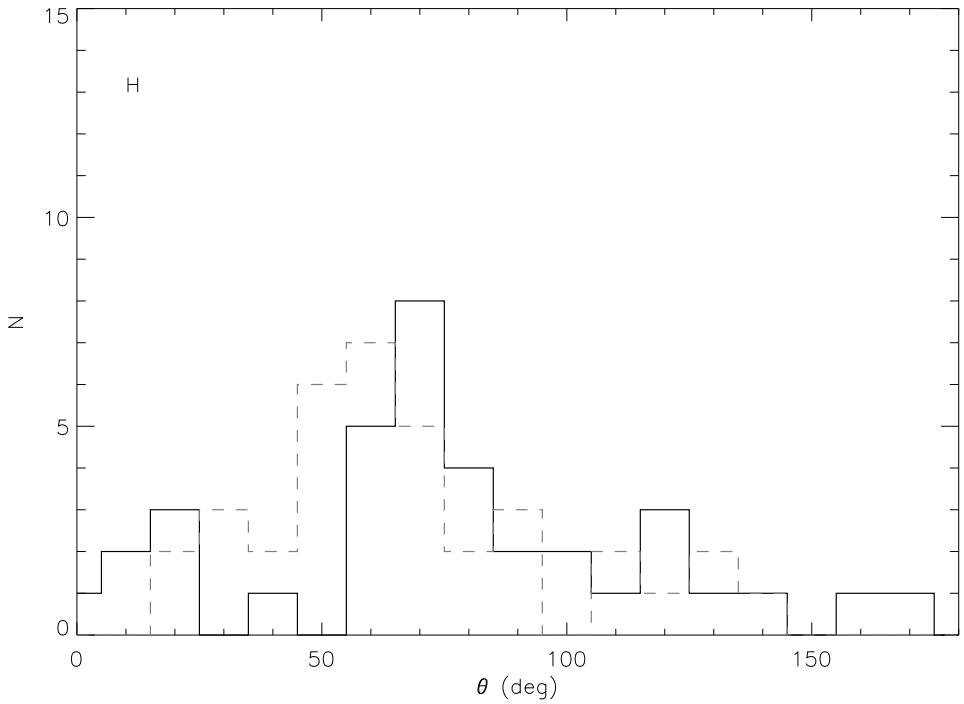

Fig. 8. Histogram of polarization angle of both matched data at *H* band. The dashed line indicates sources of N07 and solid line means our sources.

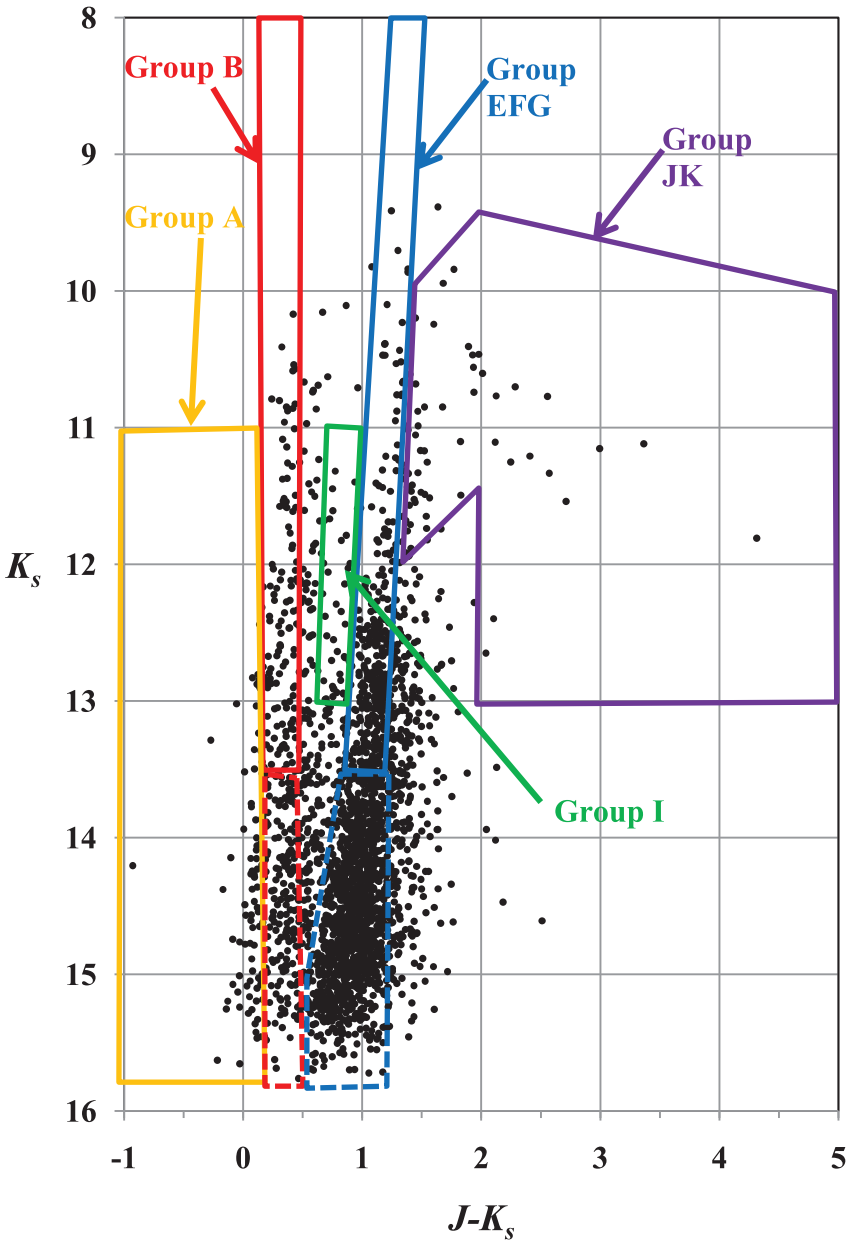

Fig. 9. Color-magnitude (J-K_s vs. K_s) diagram for our sources. The each box means that *Group A* (orange box), *Group EFG* (blue box), *Group B* (red box), *Group I* (green box), and *Group JK* (violet box).

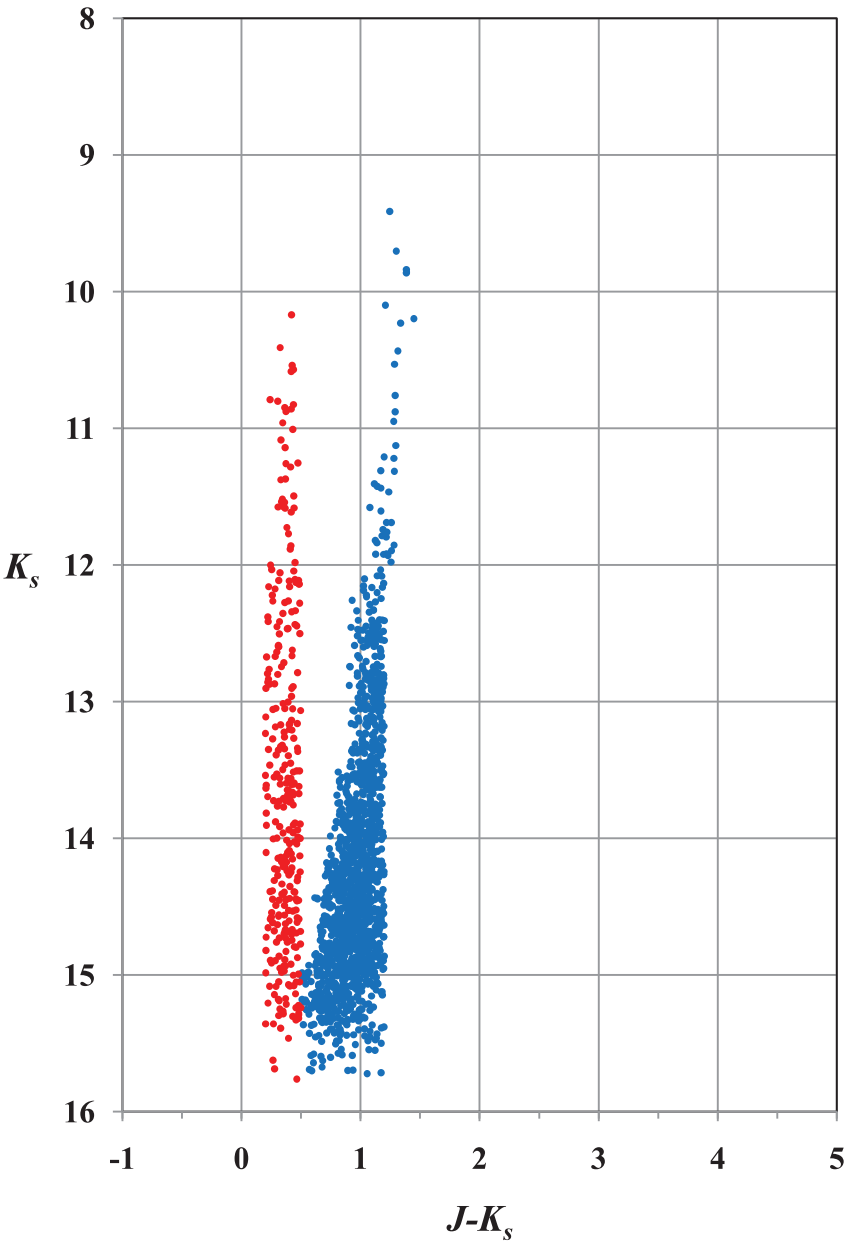

Fig. 10. Color-magnitude diagram for *Group B* and *Group EFG*. The sources are extrapolated to the boundaries.

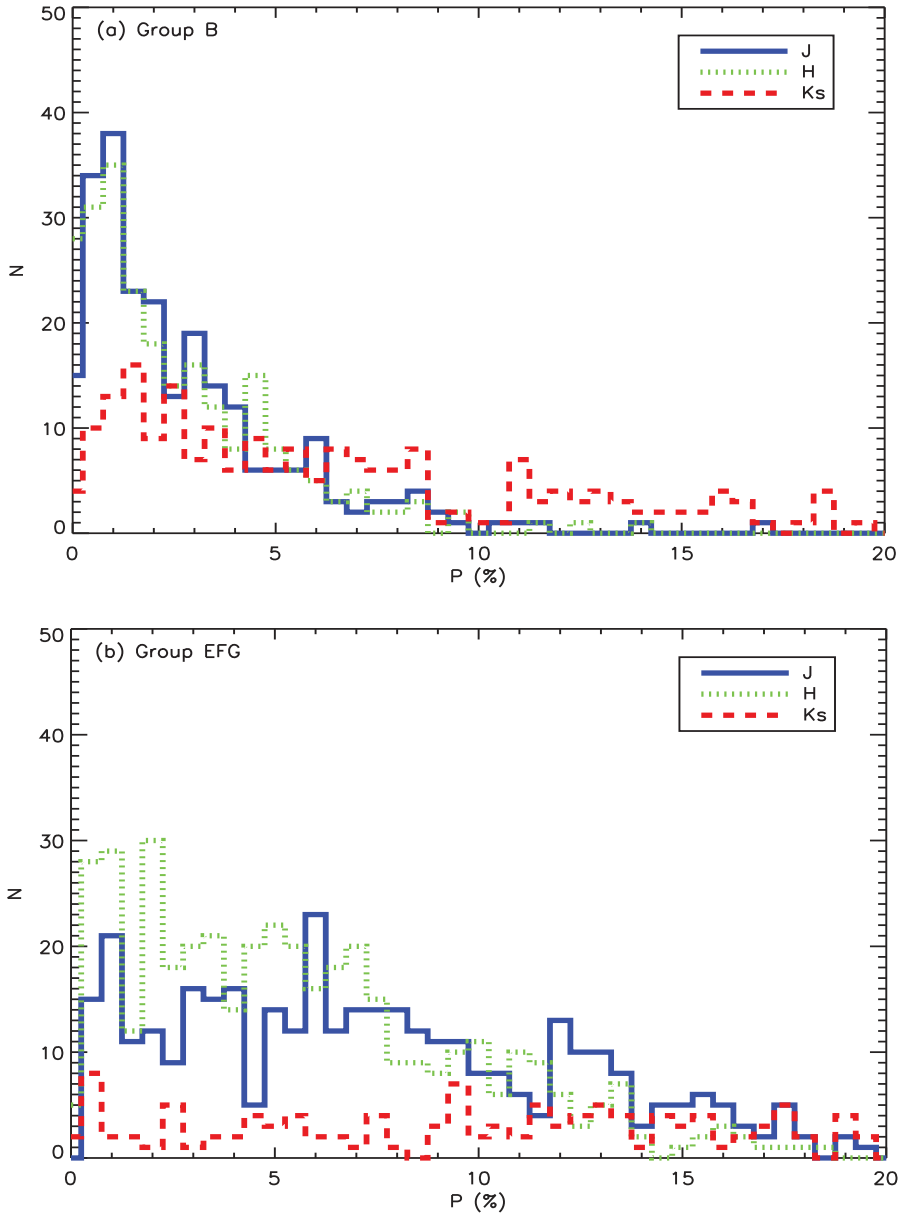

Fig. 11. (a) Histograms of polarization degree of the sources which are classified to the *Group B* for the *J*, *H*, and K_s bands. (b) Histograms of polarization degree of the sources which are classified to the *Group EFG* and $P \geq 3\sigma_P$ for the *J*, *H*, and K_s bands.

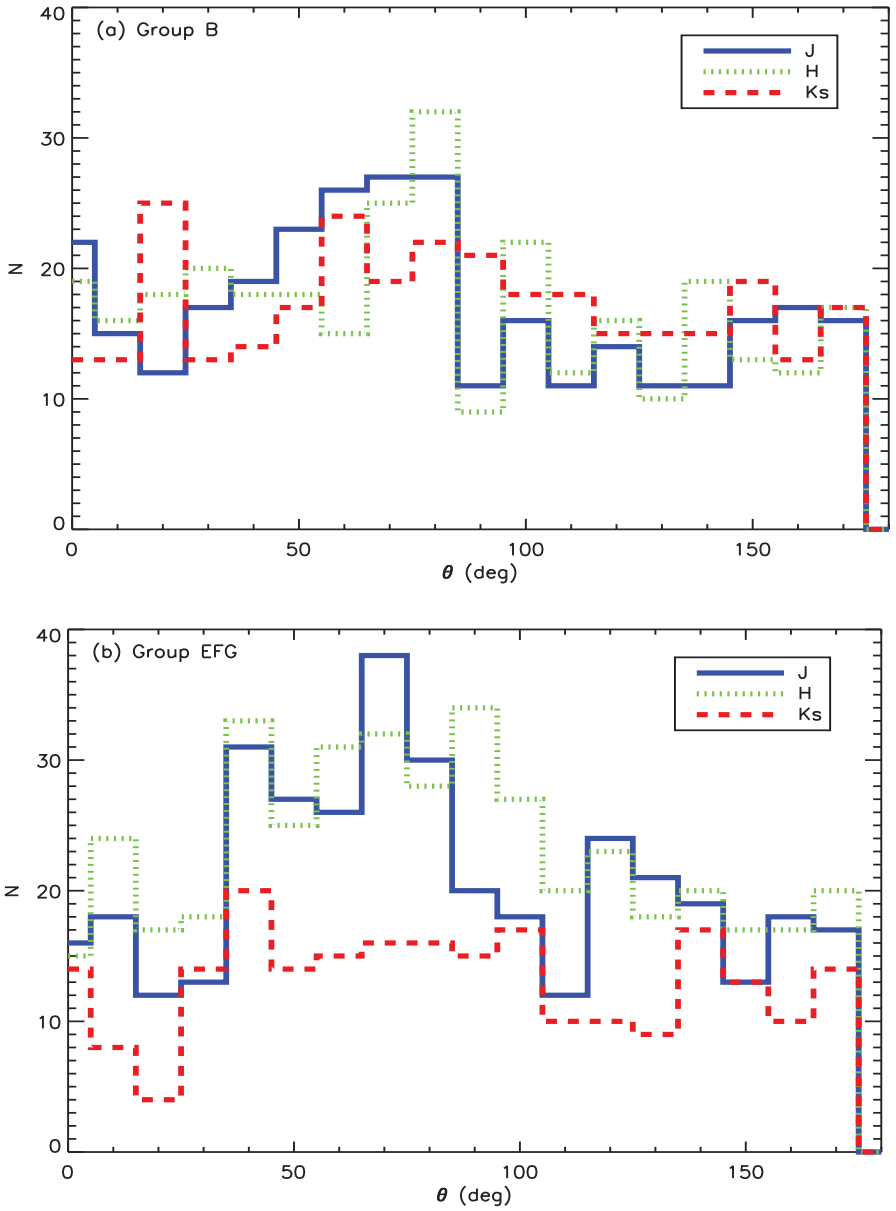

Fig. 12. (a) Histograms of polarization angle of the sources which are classified to the *Group B* for the *J*, *H*, and K_s bands. (b) Histograms of polarization angle of the sources which are classified to the *Group EFG* and $P \geq 3\sigma_P$ for the *J*, *H*, and K_s bands.

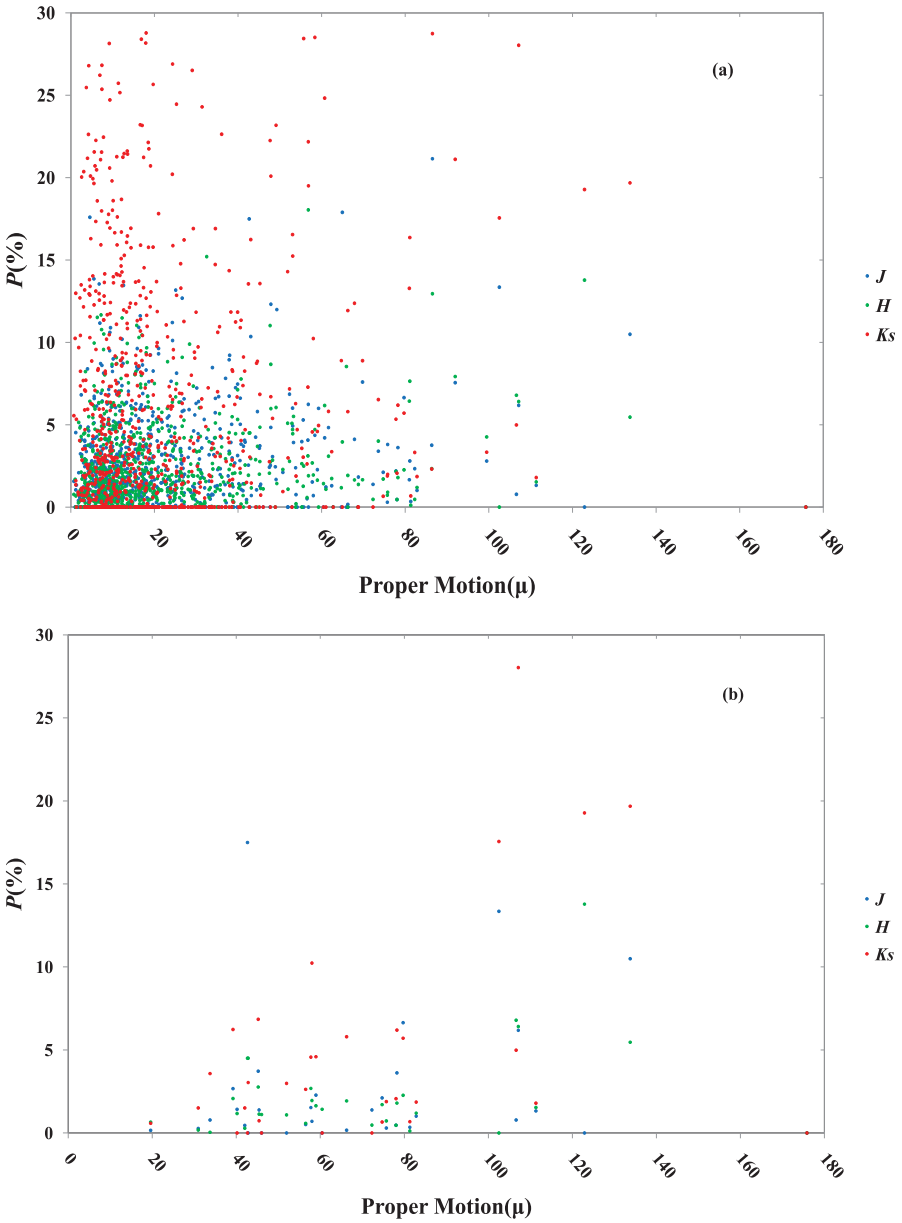

Fig. 13. (a) Plots of P and proper motion of all matched with SPM sources for the J, H, and K_s bands. (b) Plots of P and proper motion of $\mu > 3\sigma_\mu$ for the J, H, and K_s bands.

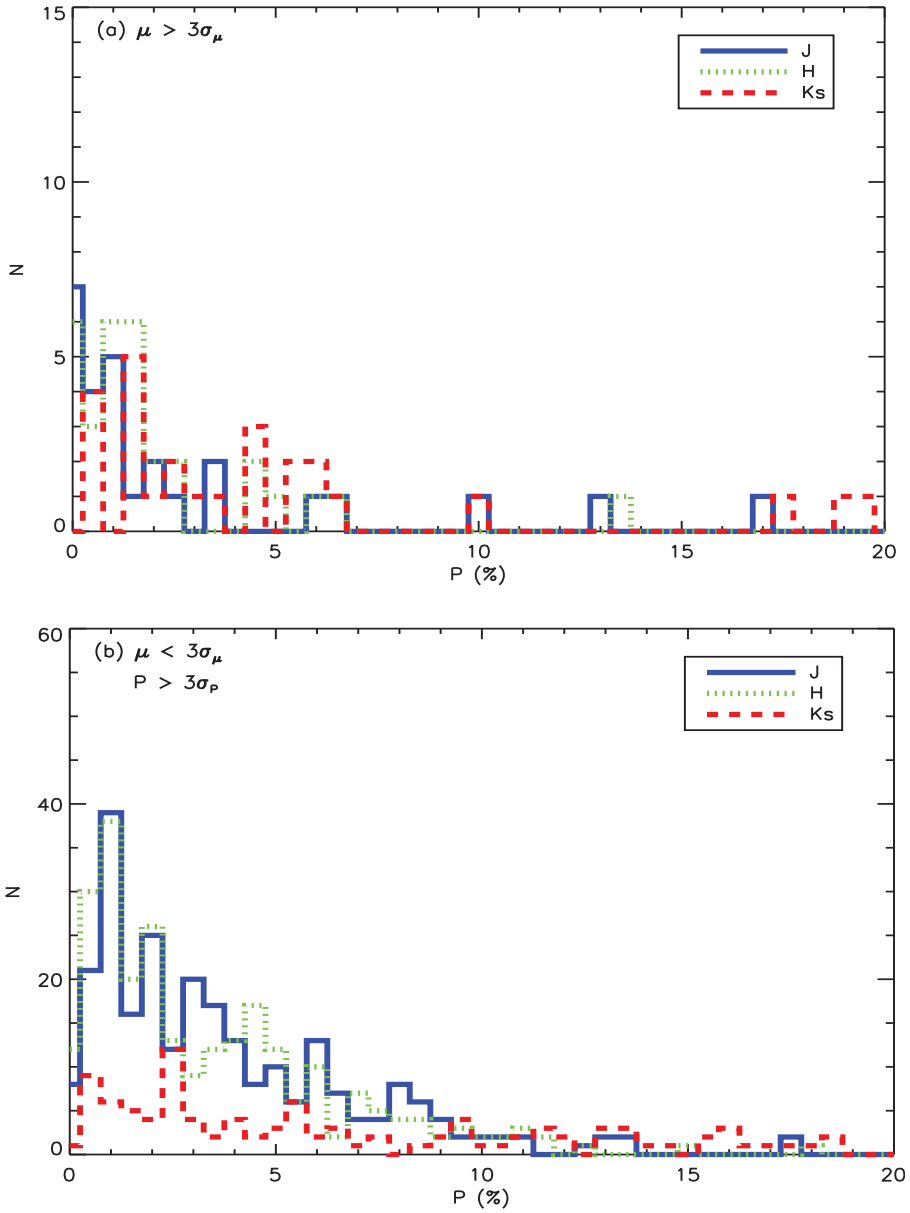

Fig. 14. (a) Histograms of polarization degree of the sources which have their proper motion $\mu > 3\sigma_\mu$ for the J, H, and K_s bands. (b) Histograms of polarization degree of the sources which have their proper motion $\mu < 3\sigma_\mu$ and $P \geq 3\sigma_P$ for the J, H, and K_s bands.

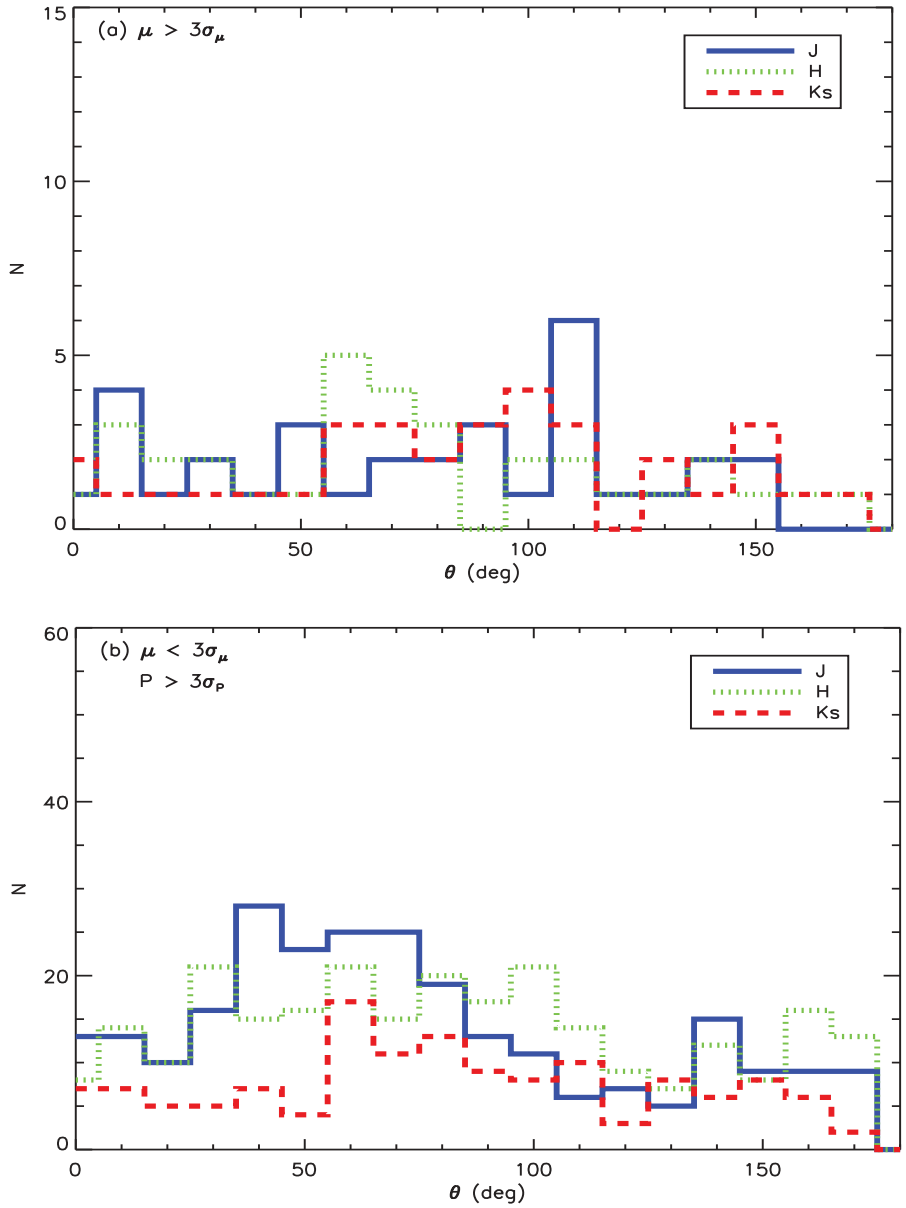

Fig. 15. (a) Histograms of polarization angle of the sources which have their proper motion $\mu > 3\sigma_\mu$ for the J, H, and K_s bands. (b) Histograms of polarization angle of the sources which have their proper motion $\mu < 3\sigma_\mu$ and $P \geq 3\sigma_P$ for the J, H, and K_s bands.

국 문 초 록

대 마젤란 성운 (LMC) 내에 위치한 30 Doradus 주변 20′ x 20′ 의 지역을 IRSF의 1.4 m 망원경을 이용하여 근적외선 파장대로 관측을 하였다. SIRIUS 편광기 (SIRPOL)을 사용하여 J, H, K_s 영역의 편광 자료를 얻었고, 별들의 Stokes 변수를 측정하여 편광 정도와 편광 각도를 계산하였다. 측광 구경을 달리 하여 편광 자료에 대한 가능한 오류들을 측정하였다. 자료의 안정성에 문제를 야기하는 우리 은하 내에 위치한 별들을 구분하기 위하여 별의 색등급도(color-magnitude diagram)와 고유운동을 이용하였다. 하지만 색등급도에서는 LMC 내에 위치한 별들과 큰 차이를 확인하지 못하여 고유운동을 통한 방법이 더 신빙성이 있다는 결론을 얻었다. 이러한 자료 분석 방법들은 LMC의 더 넓은 영역의 연구에 적용 될 것이다.

감사의 글

여러모로 부족한 저를 이끌어 주신 박수종 교수님께 진심으로 감사를 드립니다. 석사과정에 입학하기 전부터 지금까지 여러 난관에 부딪혔지만 교수님의 충고와 지도가 있었기에 이렇게 논문을 마칠 수 있었습니다. 앞으로 더 많은 시간과 노력이 필요하겠지만, 교수님께서 충고해 주시고 보여 주셨던 것들을 기억하며 꾸준히 앞으로 나아가겠습니다. 그리고 비록 많은 가르침을 받을 기회는 없었지만 참된 학자와 교육자로서 크나큰 모범이 되어 주신 김갑성 교수님, 김관혁 교수님, 김상준 교수님, 김성수 교수님, 문용재 교수님, 이동훈 교수님, 장민환 교수님, 진호 교수님, 최광선 교수님께도 감사를 드립니다.

이번 논문을 완성하기까지 큰 도움을 주셨던 천문연구원의 최민호 박사님과 서울대학교의 박원기 박사님, 그리고 서행자 박사님께도 진심으로 감사를 드립니다. 기초가 많이 부족한 저를 최선을 다해 도와주셨던 은혜를 잊지 않고, 앞으로 더욱 정진하여 큰 과학자가 되는 것으로 보답하겠습니다.

제가 지금까지 엇나가지 않고 이 길을 계속 갈 수 있었던 것은 제 주변의 좋은 친구들과 연구실 및 대학원의 선후배님들 덕분이었습니다. 연구실의 선배이자 친구로 저에게 많은 도움과 본보기가 되어 주었던 김상혁과 오희영에게 감사를 전합니다. 또한 같은 시간과 어려움을 같이 극복해 나갔던 김은빈 누나께도 감사를 전합니다. 심적으로 힘든 시기가 많이 있었지만 그 시기를 이겨나갈 수 있게 도와준 전제헌, 이대우, 서용명에게 진심으로 감사를 표합니다. 이들뿐만 아니라 우주과학과에 입학해서 지금까지 오랜 시간을 함께 해온 03 동기들이 아니었다면 지금의 나는 없었을 것입니다. 또한 저의 멘토로서 천문학자의 길을 지켜나갈 수 있게 해주신 임규희 선배님께도 진심으로 감사를 드립니다. 같은 연구실은 아니지만 연구와 공부에 대해서 많은 조언을 해주신 이재형 선배, 서정준 선배, 김현남 선배, 이용석 선배를 비롯한 분들께도 감사를 드립니다.

그리고 10년이 넘는 세월을, 비록 같은 공간에서는 아니지만 꾸준히 함께 있어왔던 나의 오랜 친구 박성욱, 오대로 에게도 감사를 전합니다.

마지막으로 지금까지 못난 자식을 헤아릴 수 없는 사랑과 믿음으로 감싸주시고 키워주셨던 어머니, 아버지께 말로 표현할 수 없는 사랑과 감사를 드립니다.

2011년 겨울

김재영 드림